IEEE Access
Multidisciplinary ⋮ Rapid Review ⋮ Open Access Journal

Received 19 July 2023, accepted 1 August 2023, date of publication 7 August 2023, date of current version 23 August 2023.

*Digital Object Identifier 10.1109/ACCESS.2023.3302323*

APPLIED RESEARCH

# Analysis of Limiting Output Capacity of Low-Speed and High-Torque Surface-Mounted Permanent Magnet Motor Considering Resistance Voltage Drop

**JIACHENG WU, GUIHONG FENG, YAN HU, BINGYI ZHANG, AND ZEYU LIU**
School of Electrical Engineering, Shenyang University of Technology, Shenyang 110870, China
Corresponding author: Guihong Feng (fenggh@sut.edu.cn)

**ABSTRACT** Drive motors in certain applications often require heavy load starting or short-time overload operation, so the limiting output capacity of the motor is worthy of attention. In this paper, the limiting output torque and input current of low-speed and high-torque external rotor surface-mounted permanent magnet synchronous motor(SMPMSM) under $i_d = 0$ and field weakening(FW) control strategies are studied considering the resistance voltage drop. Firstly, the output characteristics of SMPMSM are analyzed when the resistance is considered, and the relationships between the limiting $i_q$, limiting output torque and the electromagnetic parameters are analyzed when the $i_d = 0$ and the FW control are adopted under the voltage limit. Next, the finite element method(FEM) is used to analyze and compare the impact of different machine parameters of the SMPMSM on the limiting output torque under the two control strategies. Finally, the correctness of theoretical analysis and FEM results are verified by prototype experiments.

**INDEX TERMS** Surface-mounted permanent magnet synchronous motor, field weakening control, $i_d = 0$ control, limiting output capacity, finite element method.

## I. INTRODUCTION

Permanent magnet synchronous motor (PMSM) has the advantages of high efficiency and high power factor, so it is widely used in industry, military, agriculture and other fields [1], [2], [3], [4], [5]. In some applications where the load is uncontrollable and fluctuant, such as coal mine scraper, in order to meet the maximum possible load, the selection of the driving motor is often too large, which will not only increased costs, but also means that the motor has greater volume and weight, increasing the burden on transportation and installation. Motors with high limiting output capacity can meet the requirements of heavy load starting and short-time overload under the condition of small volume, thus saving equipment costs and reducing the space volume of the drive system. Although built-in permanent magnet synchronous motor(IPMSM) owing to its d-q axis saliency, a reluctance torque exists which will effectively improve the limiting output capacity of the motor [6], [7]. However, SMPMSM is still widely used in industrial external rotor and double-stator PMSM due to its simple processing technology and high utilization of the permanent magnets (PMs) [8], [9], [10], [11], therefore, its limiting output capacity is worthy of attention.

By the authors' best knowledge, literature shows many studies which have focused on improving the limiting output capability of PMSM. Some literature proposed better control strategies to improve the output performance of PMSM. Literature [12], [13] proposed a new direct torque control with space vector modulation(DTC-SVM) control strategy, which makes the overload capability of servo- and robot-drives PMSM significantly superior to the traditional DTC-SVM control strategy in both electric and braking modes. In reference [14], the analytical expression of current reference

The associate editor coordinating the review of this manuscript and approving it for publication was Qinfen Lu.

of IPMSM under maximum torque per ampere(MTPA) and maximum torque per volt(MTPV) control was derived without neglecting the phase resistance, and an algorithm was developed to provide the minimum current reference required by each reference torque, in addition, if the motor limiting torque cannot reach the reference torque, this algorithm can provide the maximum possible torque, thus the torque error can be minimized. Literature [15] proposed a MTPV Flux-weakening control strategy, which enables the voltage control loop management to smoothly transition the motor control track between MTPA, constant torque(CT), current and voltage limits(CVL) zones, MTPV and constant speed(CS), therefore, the maximum output capacity can be obtained under the optimal voltage or current control, moreover this control mode can take into account the resistor voltage drop and the saturation effects. At the same time, some scholars improved the torque density of PMSM by optimizing the structural parameters of the motor [16], [17], [18], [19]. Most of these literature made the motor obtain higher efficiency by optimizing the structural parameters of the motor such as pole slot matching and winding distribution so as to improve the torque density of the motor, however, these methods have relatively limited impact on the limiting output capacity of the motor. Furthermore, some scholars studied the limiting output capability of PMSM in various operating states by starting from the direction of temperature field. In literature [20], lumped heat network model was used to analyze the sensitivity of PMSM machine parameters to overload capacity under two cooling modes, direct coil cooling and cooling jacket. The results show that the sensitivity of various motor parameters to overload capacity is basically the same under the two cooling modes. Literature [21] presented a coupled electromagnetic and thermal design optimisation exercise of a traction IPMSM machine, so as to meet the required high limiting torque design objective, and the requirements of low cost and low volume.

To sum up, most scholars optimized the limiting output capacity of the motor from the control strategy or the machine parameters unilaterally. However, in actual use, the limiting output capacity of PMSM is limited by the control strategy and the machine parameters of the motor simultaneously.

In this paper, the limiting output capability of low-speed and high-torque SMPMSM considering resistance voltage drop is studied under the voltage limit of converter. Based on the electromagnetic torque equation of the motor, the influence of electromagnetic parameters of the motor on the electromagnetic torque is analyzed. The limiting electromagnetic torque of SMPMSM under $i_d = 0$ and FW control strategy is analyzed, and the influence law of electromagnetic parameters on it is summarized. By finite element method, under the condition of constant motor volume, the influences of winding turns, thickness and pole arc coefficient of permanent magnet, length of air-gap and slot width on electromagnetic parameters and the limiting output torque of SMPMSM under the two control strategies are compared and analyzed, and the difference of limiting output torque under the two control strategies with the same motor parameters is compared. The accuracy of theoretical analysis and FEM results are verified through the limiting output torque experiments of the prototype under the two control strategies. Finally, the design points of low-speed high-torque SMPMSM with requirements for limiting output capacity are summarized. The flowchart of the paper vein is shown in Fig. 1.

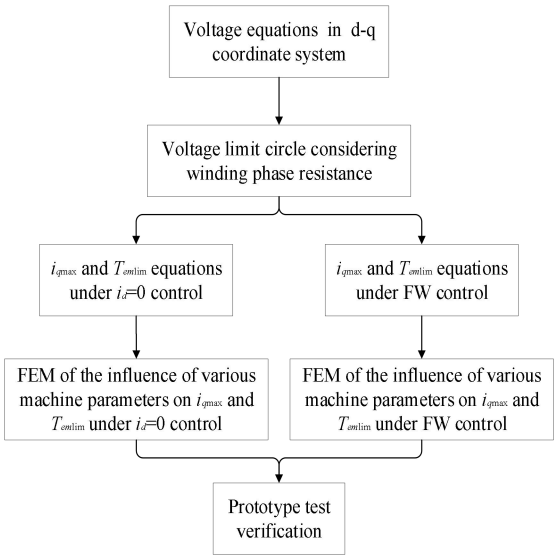


**FIGURE 1.** Flowchart of the paper vain.

## II. TORQUE ANALYSIS OF SMPMSM CONSIDERING RESISTANCE VOLTAGE DROP

At present, low-speed and high-torque PMSM often adopt vector control strategy. This control strategy can decoupled strong coupling torque current and excitation current in d-q coordinate system, thereby providing better control performance for PMSM. The voltage equations of PMSM operating stably at synchronous speed in the d-q coordinate system [22] are as follows:

$$\begin{cases} v_d = R_s i_d - \omega_e L_q i_q \\ v_q = R_s i_q + \omega_e L_d i_d + \omega_e \lambda_{pm} \end{cases} \tag{1}$$

where $v_d$, $v_q$, $i_d$, $i_q$, $L_d$ and $L_q$ are representing d-q axis voltages, currents and inductances, $\lambda_{pm}$ is the PM flux linkage, $R_s$ is the winding phase resistance, $\omega_e$ is the electrical speed.

For PMSM operating at constant speed, $v_d$ and $v_q$ will increase with the increase of $i_d$ and $i_q$ until reaching the voltage and current limits on the DC side of the inverter in the converter [14]. The current limit of the converter can be adjusted by changing its capacity, while the voltage limit is related to the power supply line which is generally a constant value. This results in the limiting terminal voltage of the motor being fixed, so the maximum current that the motor can input is mainly limited by this limiting voltage.

The voltage restriction can be expressed as (2):

$$\sqrt{v_d^2 + v_q^2} = v_s \le v_{\lim} = \frac{V_c}{\sqrt{6}} \tag{2}$$

where $v_s$, $v_{\lim}$ and $V_c$ are representing the terminal voltage of the motor, the limiting terminal voltage of the motor, and maximum voltage on the DC side of the inverter.

Equations (1) and (2) can be represented in diagram phasor as shown in Fig. 2.

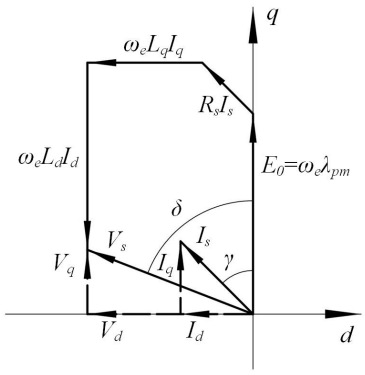


**FIGURE 2.** Phasor diagram in dq-axis.

For SMPMSM, the d and q-axis inductances are approximately equal, that is:

$$L_d = L_q = L_s \tag{3}$$

where $L_s$ is the synchronous inductance of the motor.

By substituting (1) into (2), the terminal voltage equation of SMPMSM in steady state can be obtained:

$$v_s = \sqrt{(-X_s i_q + R_s i_d)^2 + (X_s i_d + e_0 + R_s i_q)^2} \tag{4}$$

where $X_s = \omega_e L_s$ is the synchronous reactance, $e_0 = \omega_e \lambda_{pm}$ is the no-load back electromotive force.

The $\omega_e$ of low-speed and high-torque PMSM is generally low, resulting in a small $X_s$, and the input current of the motor is high when the motor is running at the limiting output condition, so the resistance voltage drop can not be ignored in this condition. By substituting $v_{\lim}$ into (4) and organizing it, the voltage limit circle equation of SMPMSM can be obtained:

$$\left(i_d + \frac{X_s e_0}{R_s^2 + X_s^2}\right)^2 + \left(i_q + \frac{e_0 R_s}{R_s^2 + X_s^2}\right)^2 = \frac{v_{\lim}^2}{R_s^2 + X_s^2} \tag{5}$$

Fig. 3. shows a comparison of voltage limit circles when winding phase resistance is neglected and considered.

As can be seen from Fig. 3, compared with the voltage limit circle neglecting the resistance, the center of the voltage limit circle considering the resistance will shift from the X-axis to the lower right, and the radius of the circle will also slightly decrease, so the maximum $i_q$ that can be input the motor will decrease.

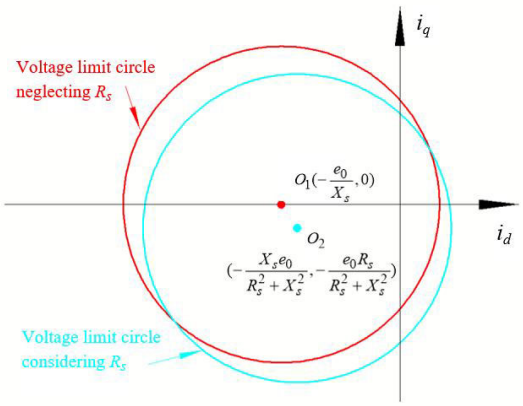


**FIGURE 3.** Comparison of voltage limit circles.

For SMPMSM, the electromagnetic torque can be expressed as (6):

$$\begin{aligned} T_{em} &= \frac{3}{2} p \lambda_{pm} i_q \\ &= \frac{3}{2\omega_m} e_0 i_q \end{aligned} \tag{6}$$

The relationship between mechanical and electrical speeds is expressed as:

$$\omega_m = \frac{\omega_e}{p} \tag{7}$$

where $\omega_m$ is the mechanical speed and $p$ is the pair of poles.

According to (6), when the motor runs at a constant speed, the electromagnetic torque of the motor is only proportional to $e_0$ and $i_q$. Therefore, when SMPMSM outputs the limiting torque, the $i_q$ input into the motor should be the limiting value under the voltage limit.

For low-speed and high-torque PMSM, because the $\omega_m$ and $\omega_e$ are low, so the proportion of stator iron loss and stray loss is very small, so there is:

$$T_{em} \approx T_{out} \tag{8}$$

## III. LIMITING OUTPUT TORQUE ANALYSIS OF SMPMSM UNDER $i_d = 0$ AND FW CONTROL STRATEGY

For SMPMSM, $i_d = 0$ control is also MTPA control, which can generate maximum electromagnetic torque with the minimum current and minimize the heat generation of the motor [23]. While FW control can make the SMPMSM input more current to improve the limiting output capacity. Therefore, for SMPMSM, $i_d = 0$ and FW control are the most commonly used control strategies. This section analyzes the limiting output torque of SMPMSM in the two control strategies.

### A. LIMITING OUTPUT TORQUE ANALYSIS OF SMPMSM UNDER $i_d = 0$ CONTROL

For SMPMSM, the constant torque curves (CTC) at constant speed and $i_d = 0$ control trajectory under the limiting terminal

voltage are shown in Fig. 4, according to equation (6), they are a series of parallel lines proportional to $i_q$.

Point A in Fig. 4. is the maximum current that the motor can input under the limiting terminal voltage when the $i_d = 0$ control strategy is adopted.

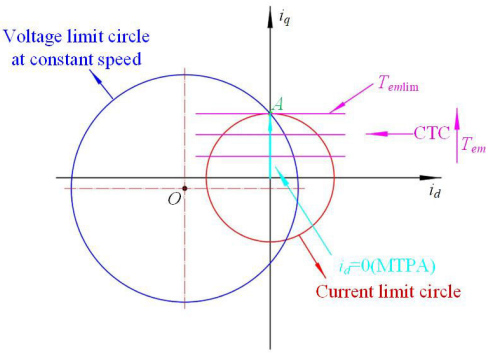


**FIGURE 4.** Constant torque curves and $i_d = 0$ control trajectory.

By substituting $i_d = 0$ into formula (5), the current at point A can be expressed as:

$$i_{s\max} = i_{q\max} = \frac{\sqrt{v_{\lim}^2\left(R_s^2 + X_s^2\right) - X_s^2 e_0^2} - e_0 R_s}{R_s^2 + X_s^2} \tag{9}$$

Since $v_{\lim}$ is a constant value, there is $i_{q\max} = f(e_0, X_s, R_s)$, and their relation surfaces are shown in Fig. 5. It can be seen that as $R_s$, $X_s$, and $e_0$ increase, $i_{q\max}$ shows a downward trend. This is because when $R_s$ and $X_s$ increase, the impedance voltage of the motor winding will increase when the same current is applied. While, the increase of $e_0$ will make the difference between $v_{\lim}$ and $e_0$ to decrease, resulting in a smaller value left for the winding impedance voltage, so $i_{q\max}$ decreases.

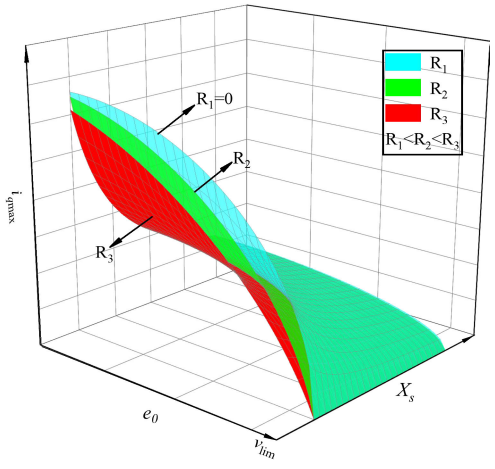


**FIGURE 5.** Relation surfaces between $i_{qmax}$, $e_0$, $R_s$ and $X_s$ under $i_d = 0$ control.

When the machine parameters and rated speed of the motor are fixed, it can be seen from equation (6) that, for SMPMSM, the output torque is proportional to $i_q$, so when the current is located at point A, the maximum $i_q$ that the motor can input, the SMPMSM can obtain the limiting output torque. By substituting (9) into (6), the limiting output torque of SMPMSM under the $i_d = 0$ control can be written:

$$T_{em\lim} = \frac{3}{2\omega_m} \frac{e_0\sqrt{v_{\lim}^2\left(R_s^2 + X_s^2\right) - X_s^2 e_0^2} - e_0^2 R_s}{R_s^2 + X_s^2} \tag{10}$$

Since $v_{\lim}$ and $\omega_m$ are both constant, so $T_{em\lim} = f(R_s, X_s, e_0)$, their relation surfaces are shown in Fig. 6. It can be seen that as $R_s$ and $X_s$ increase, $T_{em\lim}$ shows a downward trend, which is because as $R_s$ and $X_s$ increase, the $i_{q\max}$ that the can be input the motor decreases. As $e_0$ increases, $T_{em\lim}$ first increases and then decreases, combined with Fig. 5, it can be seen that this is because with the increase of $e_0$, the rate of $i_{q\max}$ decreasing gradually exceeds the rate of $e_0$ increasing. Therefore, there is a specific $e_0$ value that can enable $T_{em\lim}$ to reach its maximum value, that is:

$$\frac{\partial T_{em\lim}}{\partial e_0} = 0$$

$$e_0 = \frac{v_{\lim}\sqrt{2(X_s^2 + R_s^2)}}{2X_s} \tag{11}$$

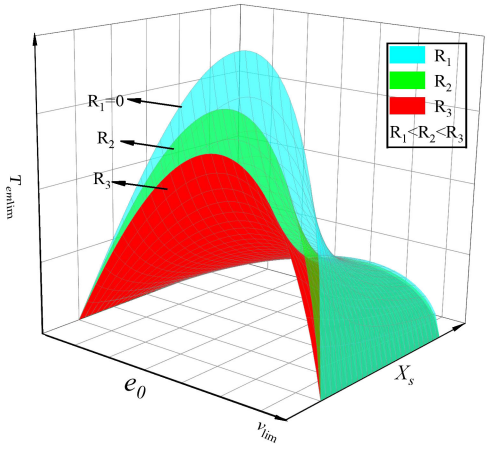


**FIGURE 6.** Relation surfaces between $T_{emlim}$, $e_0$, $R_s$ and $X_s$ under $i_d = 0$ control.

From the above analysis, it can be seen that under $i_d = 0$ control, in order to obtain a larger limiting output torque of the SMPMSM, it is necessary to minimize $X_s$ and $R_s$ as much as possible and select an appropriate $e_0$ value.

### B. LIMITING OUTPUT TORQUE ANALYSIS OF SMPMSM UNDER FW CONTROL

For SMPMSM, the CTC at constant speed and the FW control trajectory under the limiting terminal voltage are shown in Fig. 7. It can be seen that there are countless current vectors on the constant torque curve that can meet this certain electromagnetic torque, but the minimum current value will be obtained only when the end point of the current vector

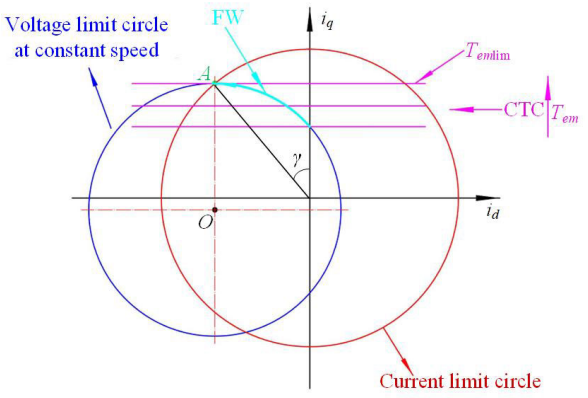


**FIGURE 7.** Constant torque curves and FW control trajectory.

is located on the voltage limit circle. Therefore, this paper chooses this weak magnetic control strategy, that is, the motor terminal voltage is kept at the limit value. This control strategy is implemented according to literature [15].

Point A in Fig. 7. shows the $i_{q\max}$ that the motor can input when the FW control strategy is adopted. The expression of the current at point A is:

$$\begin{cases} i_d = -\dfrac{e_0 X_s}{R_s^2 + X_s^2} \\ i_{q\max} = \dfrac{v_{\lim}\sqrt{R_s^2 + X_s^2} - e_0 R_s}{R_s^2 + X_s^2} \\ i_s = \sqrt{i_d^2 + i_{q\max}^2} \end{cases} \tag{12}$$

The current lead angle $\gamma$ of point A can be expressed as:

$$\begin{aligned} \gamma &= \arctan\frac{|i_d|}{i_{q\max}} \\ &= \arctan\left(\frac{e_0 X_s}{v_{\lim}\sqrt{R_s^2 + X_s^2} - e_0 R_s}\right) \end{aligned} \tag{13}$$

Similarly, since $v_{\lim}$ is a constant value, there is $i_{q\max} = f$ ($e_0$, $X_s$, $R_s$), and their relationship surfaces are shown in Fig. 8. It can be seen that when $R_s$, $X_s$, and $e_0$ increase, $i_{q\max}$ still shows a downward trend. However, different from $i_d = 0$ control, $i_{q\max}$ is less sensitive to $e_0$ under FW control, and the smaller $R_s$ and $X_s$, the lower this sensitivity. This is because the input $i_{q\max}$ under FW control is less affected by the difference between $v_{\lim}$ and $e_0$, and mainly depends on the position and radius of the voltage limit circle.

Also according to equation (6), when the current is located at point A, the SMPMSM can obtain the maximum $i_q$ value, the SMPMSM can also obtain the limiting output torque. By substituting (12) into (6), the limiting output torque of SMPMSM under the FW control can be written:

$$T_{em\lim} = \frac{3}{2\omega_m} \times \frac{e_0 v_{\lim}\sqrt{\left(R_s^2 + X_s^2\right)} - e_0^2 R_s}{R_s^2 + X_s^2} \tag{14}$$

Also, since the $v_{\lim}$ and $\omega_m$ are both constant, there is $T_{em\lim} = f$ ($R_s$, $X_s$, $e_0$), and their relation surfaces are shown in Fig. 9. It can be seen that when $R_s$ and $X_s$ increase,

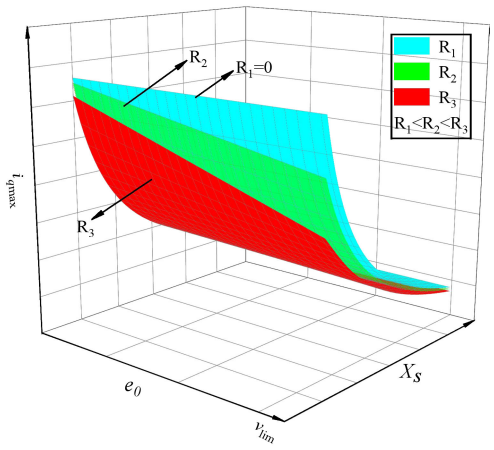


**FIGURE 8.** Relation surface between $i_{qmax}$, $e_0$, $R_S$ and $X_S$ under FW control.

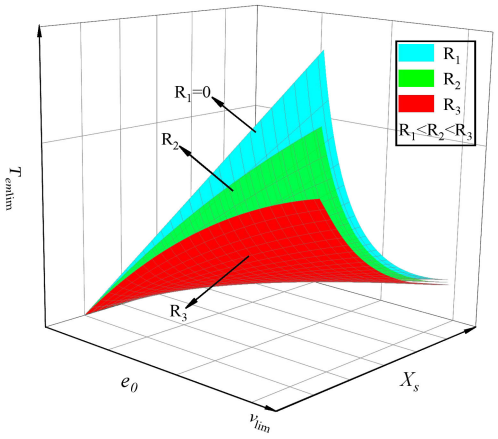


**FIGURE 9.** Relation surface between $T_{emlim}$, $e_0$, $R_S$ and $X_S$ under FW control.

$T_{em\lim}$ shows a downward trend. Due to the $R_s$ of low-speed high-torque motor is small, and $X_s$ is not very small, therefore, within the actual $X_s$ and $R_s$ range, $T_{em\lim}$ increases with the increase of $e_0$, combined with Fig. 8, this is because as $e_0$ increases, although $i_{q\max}$ decreases, its rate of decrease is much lower than the rate of $e_0$ increase.

In summary, under FW control, $X_s$ and $R_s$ should be reduced as much as possible and $e_0$ should be increased as much as possible so that the SMPMSM can obtain a larger limiting output torque.

## IV. INFLUENCE OF MACHINE PARAMETERS ON LIMITING OUTPUT TORQUE UNDER $i_d = 0$ AND FW CONTROL

In this section, FEM analysis is carried out on the existing prototype to analyze the influence of different machine parameters on the limiting output torque under $i_d = 0$ and FW control with or without considering resistance. The prototype is applied to the belt conveyor, and its main parameters and finite element models are shown in Table 1 and Fig. 10. respectively.

**TABLE 1. Main parameters of the prototype.**

| Item | Unit | Value |
|---|---|---|
| Rated power | kW | 160 |
| Rated voltage | V | 1140 |
| Rated speed | r/min | 76.5 |
| Core length | mm | 600 |
| Length of air-gap($\delta$) | mm | 2 |
| Number of poles/slots | - | 60/72 |
| Outside diameter of stator | mm | 880 |
| Outside diameter of rotor | mm | 1000 |
| Thickness of PM($h_M$) | mm | 10 |
| Slot width($b_s$) | mm | 19.5 |
| Pole arc coefficient of PM($\alpha_c$) | - | 0.75 |
| Number of turns($N_s$) | - | 10 |
| Phase resistance($R_s$) | Ω | 0.185 |
| Synchronous reactance($X_s$) | Ω | 2.925 |

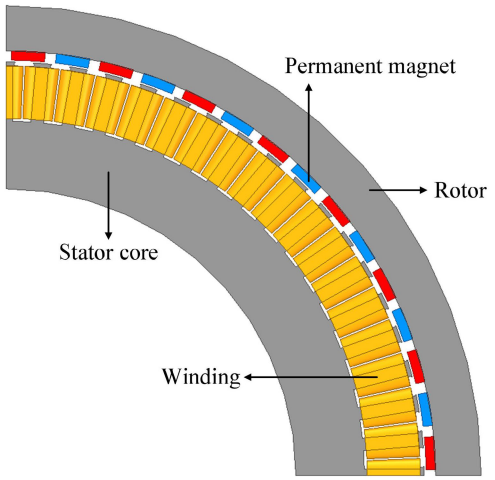


**FIGURE 10. Finite element model of prototype.**

It is only meaningful to compare the limiting output capacity of SMPMSM under the same volume, therefore, it is necessary to consider how to adjust $e_0$, $X_s$ and $R_s$ under the condition of constant motor volume, in order to obtain greater limiting output torque of the SMPMSM. It is acknowledged that some machine parameters, such as rotor thickness and stator yoke thickness, have low magnetic density under the condition of satisfying mechanical strength, so the have little influence on $e_0$, $X_s$ and $R_s$. While the adjustment of $N_s$, $h_M$, $\alpha_c$, $\delta$ and $b_s$ is an effective way to adjust the reluctance, flux and other parameters of the motor magnetic circuit so as to affect $e_0$, $X_s$ and $R_s$, however, changing these parameters will affect $e_0$, $X_s$ and $R_s$ simultaneously. Analytical expressions are helpful for analyzing the influence trends of these machine parameters on $e_0$, $X_s$ and $R_s$. Their expressions are shown in Equations (15)-(17) respectively.

$$e_0 = 4.44 f N K_{dp} \Phi_0 \tag{15}$$

where $f$ is the rated frequency, $N$ is the number of series turns of each phase winding, $K_{dp}$ is the winding factor, $\Phi_0$ is the fundamental wave flux of each pole generated by PM.

$$R_s = \rho \frac{2 l_{av} N}{a \pi N_t k_1 h_1} \tag{16}$$

where $\rho$ is the resistivity of the copper wire, $l_{av}$ is the average half-turn length of the winding coil, $a$ is the number of parallel branches, $N_t$ is the number of parallel roots of the coil, $k_1$ and $h_1$ are the width and thickness of the copper wire respectively.

$$\begin{aligned} X_s &= \omega_e L_s \\ &= \omega_e \times (L_m + L_\sigma) \\ &= \frac{2 \omega_e \mu_0 l_{ef} N^2}{pq} (\lambda_m + \lambda_s + \lambda_h + \lambda_e) \end{aligned} \tag{17}$$

where $L_m$ and $L_\sigma$ are the main inductance and leakage inductance of the motor respectively, $\mu_0$ is the vacuum permeability, $l_{ef}$ is the armature calculation length, $\lambda_m$, $\lambda_s$, $\lambda_h$, $\lambda_e$ are the main magnetic circuit specific permeability, slot ratio leakage permeability, harmonic ratio leakage permeability and end ratio leakage permeability.

In this section, the FEM is used to analyze the influence of these parameters on the limiting $i_q$ and limiting output torque of the prototype in Table 1 under the two control strategies, and combined with the above equations, the FEM comparison results are explained in detail.

### A. THE EFFECT OF NUMBER OF TURNS ON LIMITING OUTPUT TORQUE

Adjusting the $N_s$ of SMPMSM will simultaneously change $e_0$, $R_s$, and $X_s$. An excessively small number of $N_s$ will cause a sharp increase in rated current, while an excessively large $N_s$ will lead to $e_0$ greater than $v_{\text{lim}}$, these situations are unacceptable in motor design, so the $N_s$ is taken within the range of 7-10 for analysis. Fig. 11. shows the variation trend of the main electromagnetic parameters of the prototype when $N_s$ changes.

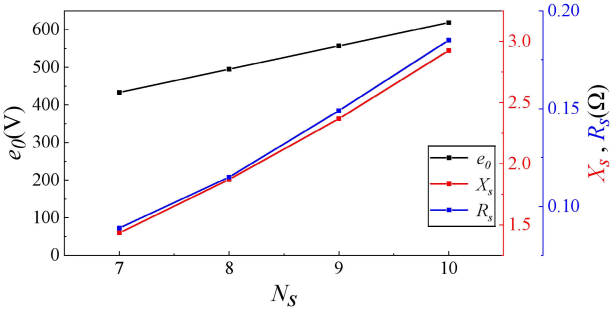


**FIGURE 11. $e_0$, $R_s$, $X_s$ at different $N_s$.**

Since the excitation parameters of PM are unchanged, with the increase of $N_s$, the number of series turns of each phase winding also increases. According to equations (15) and (17), $e_0$ linearly increase as winding flux increases with

the increase of $N_s$, while $X_s$ is quadratic to $N_s$. Because the stator slot is unchanged, when the $N_s$ increases, in order to meet the appropriate slot filling rate, the copper wire width $k_1$ remains unchanged, but the copper wire thickness $h_1$ will decrease accordingly, which will lead to a smaller cross-sectional area of each turn winding. According to equation (16), in this case $R_s$ also increases approximately linearly. In addition, it is worth noting that when the $N_s$ changes, the current lead angle $\gamma$ at $i_{q\max}$ will also change, as shown in Fig. 12.

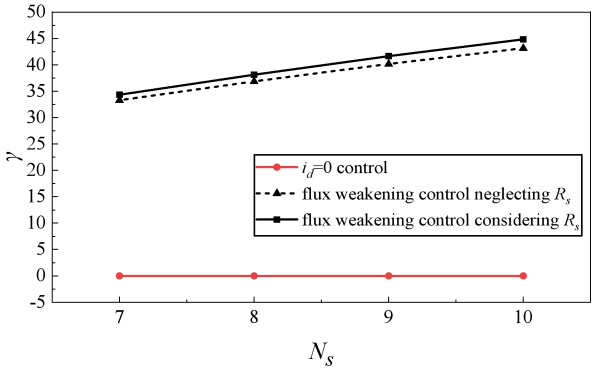


**FIGURE 12.** Current lead angle $\gamma$ at different $N_s$.

Although $i_{q\max}$ can better reflect the impact on the limiting output torque, it is still necessary to determine $\gamma$ to obtain the $i_s$ of SMPMSM under the voltage limit, and $i_q$ needs to be adjusted by $i_s$ and $\gamma$ in the finite element software, so the analysis of $\gamma$ is necessary. It can be seen that whether resistance is considered or not, the current lead angle $\gamma$ is always 0° under $i_d = 0$ control, while under FW control, according to equation (13), when resistance is not considered, as $e_0$ gets closer to $v_{\lim}$, the current lead angle $\gamma$ at $i_{q\max}$ will get closer to 45°. However, when considering the resistance, due to the shift of the voltage limit circle, the current lead angle $\gamma$ at $i_{q\max}$ is slightly greater than 45°.

When the $N_s$ changes, the maximum current curves are shown in Fig. 13. It is also worth noting that $i_{q\max}$ and $i_s$ in Fig. 13. correspond one-to-one to $\gamma$ in Fig. 12. Since $e_0$, $X_s$ and $R_s$ all increase with the increase of the $N_s$, according to equations (9) and (12), it is not conducive to improving the $i_{q\max}$ that the motor can input. Therefore, under the two control strategies, the $i_{q\max}$ decreases with the increase of $N_s$. It is worth noting that under FW control, although the current lead angle $\gamma$ increases with the increase of $N_s$, the difference between $i_s$ and $i_q$ becomes smaller due to $i_{q\max}$ has a greater tendency to decrease. In addition, although $R_s$ also increases with the increase of $N_s$, but the rate of current reduction is faster, making the resistance voltage drop smaller, so the current difference becomes smaller when considering and neglecting resistance. It's worth noting that when the unit current is passed into the winding, the increase of $N_s$ will lead to the increase of the stator flux, which will produce a larger electromagnetic torque on the rotor, so the rated current required at the rated torque can be reduced. However, because the winding resistance increases, the motor thermal load is almost unchanged at the rated operating point. The trend of current variation in Fig. 13. is consistent with that in Fig. 5. and Fig. 8.

When the $N_s$ changes, the limiting output torque curves is shown in Fig. 14.

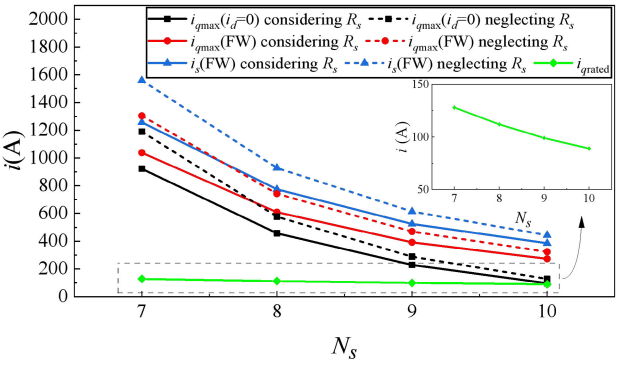


**FIGURE 13.** Maximum current curves at different $N_s$.

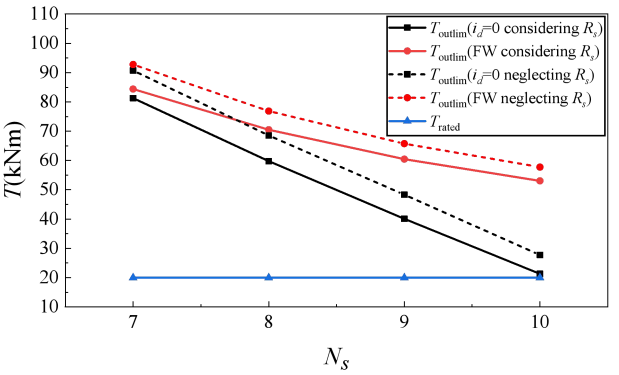


**FIGURE 14.** Limiting output torque curves at different $N_s$.

As $N_s$ increases, the limiting output torque under both control strategies decreases, this is because the rate at which $e_0$ increases is less than the rate at which $i_{q\max}$ decreases, and the limiting torque is proportional to $e_0$ and $i_{q\max}$. But the limiting output torque under FW control decreases more slowly, and the larger the $N_s$ is, the larger the limiting output torque of FW control is than that of $i_d = 0$ control. This is because $e_0$ is the same in both control strategies when the $N_s$ increases, but the difference between the their $i_{q\max}$ becomes larger. The variation trend of the torque in Fig. 14. is consistent with that in Fig. 6. and Fig. 9.

According to the analysis of Fig. 11-14, when $N_s$ increases, although the increase of $e_0$ is conducive to improving the limiting output torque, due to the voltage limit of the inverter, the $i_{q\max}$ that the motor can input decreases, and because $X_s$ and $R_s$ increase at the same time, the decrease of $i_{q\max}$ is much greater than the increase of $e_0$, as a result, the limiting output torque decreases with the increase of the $N_s$, while under FW

control can improve the $i_{q\max}$, therefore, the limiting output torque of the SMPMSM under FW control is greater than that under $i_d = 0$ control. Moreover, when the resistance is ignored, the SMPMSM can obtain a larger $i_{q\max}$, so the limiting output torque is greater than when the resistance is considered.

### B. THE EFFECT OF THICKNESS OF PM ON LIMITING OUTPUT TORQUE

$e_0$ and $X_s$ will change by adjusting the $h_M$ of PM, but $R_s$ is unaffected. Fig. 15. shows the variation trend of the main electromagnetic parameters of the prototype when $h_M$ changes.

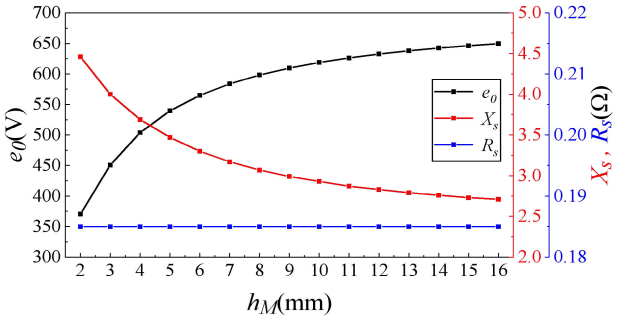


**FIGURE 15.** $e_0$, $R_s$, $X_s$ at different $h_M$.

When the $h_M$ increases, the magnetomotive force of each pole increases, which leads to the increase of the no-load operating point of PM, this will increase the magnetic flux produced by the permanent magnet, which, according to equation (15) will increase $e_0$. However, the increase trend of $e_0$ slows down with the saturation of stator core. In addition, as the $h_M$ increases, the equivalent air gap of the motor increases and the saturation degree of the iron core increases. As the saturation degree of magnetic circuit increases, the specific permeability of the main magnetic circuit will decrease, resulting in the decrease of $X_s$, furthermore as the saturation degree increases, the rate of $X_s$ reduction decreases. When the $h_M$ changes, the current lead angle $\gamma$ at $i_{q\max}$ is shown in Fig. 16.

Under $i_d = 0$ control, the current lead angle $\gamma$ remains at 0 °, while under FW control, the current lead angle $\gamma$ increases with the increase of $h_M$, this is also caused by increasing $e_0$, and the trend of increasing $\gamma$ is consistent with the trend of increasing $e_0$. The same thing as before, the current lead angle $\gamma$ eventually approaches 47° when the resistance is considered, while the current lead angle $\gamma$ finally approaches 45° when the resistance is ignored.

When the $h_M$ changes, the maximum current curves are shown in Fig. 17. It can be seen that under $i_d = 0$ control, the $i_{q\max}$ decreases with the increase of $h_M$, while under FW control, the $i_{q\max}$ increases and the increase trend becomes slow. In addition, higher current can be obtained in both control modes without regard to resistance. Furthermore, because

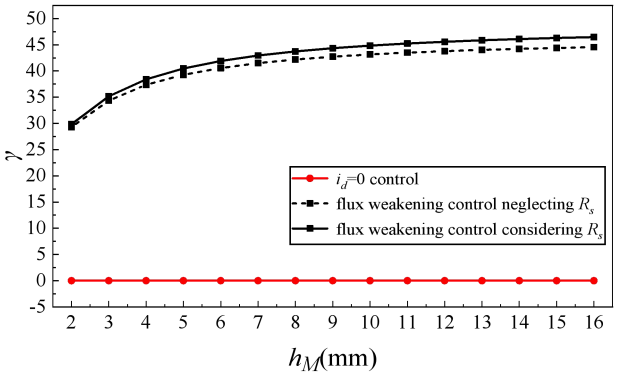


**FIGURE 16.** Current lead angle $\gamma$ at different $h_M$.

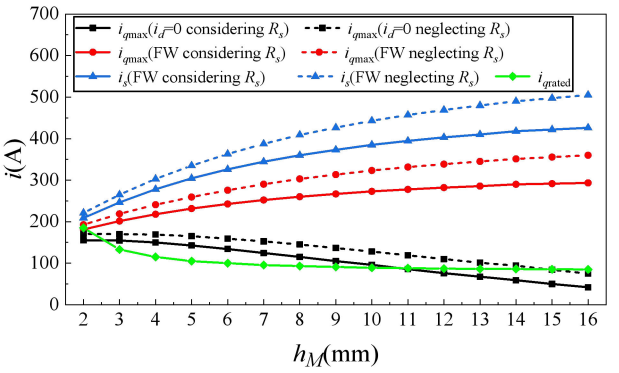


**FIGURE 17.** Maximum current curves at different $h_M$.

the current lead angle $\gamma$ at $i_{q\max}$ is almost unchanged when the $h_M$ increases to a certain extent, the difference between $i_s$ and $i_{q\max}$ gradually increases with the increase of $i_{q\max}$. Moreover, when the $h_M$ increases, the intensity of the air gap magnetic field increases due to the enhancement of the excitation field of the PMs, the rated $i_q$ required at rated torque decreases, however, with the deepening of saturation degree, the rated $i_q$ gradually becomes stable. It is worth noting that when the $h_M$ is too large, the input $i_{q\max}$ of the motor cannot reach the rated value, in this case, for $i_d = 0$ control, the motor cannot output rated torque, while for FW control, the motor has entered the FW range when it outputs rated torque.

When the $h_M$ changes, the limiting output torque curves are shown in Fig. 18. With the increase of $h_M$, the limiting output torque under $i_d = 0$ control first increases and then decreases. This is because $e_0$ of the motor increases with the increase of $h_M$ and the increase rate gradually slows down, while the $i_{q\max}$ of the motor decreases almost linearly, therefore, when the $h_M$ is small, the limiting output torque of the SMPMSM tends to increase with the increase of $h_M$, then, when the increasing trend of $e_0$ slows down, the decrease of $i_{q\max}$ plays a decisive role, which leads to the decrease of the limiting output torque. When $e_0$ is within the range of $0.75\sim0.85v_{\lim}$ by adjusting the $h_M$, the SMPMSM can achieve a larger limiting output torque. However, under the

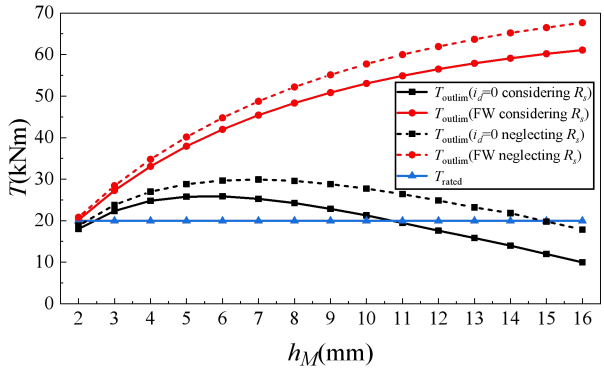


**FIGURE 18.** Limiting output torque curves at different $h_M$.

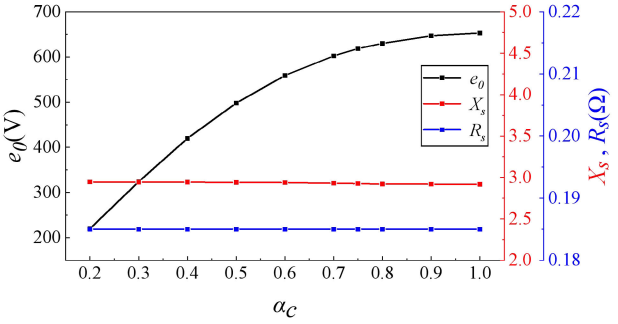


**FIGURE 19.** $e_0$, $R_s$, $X_s$ at different $\alpha_c$.

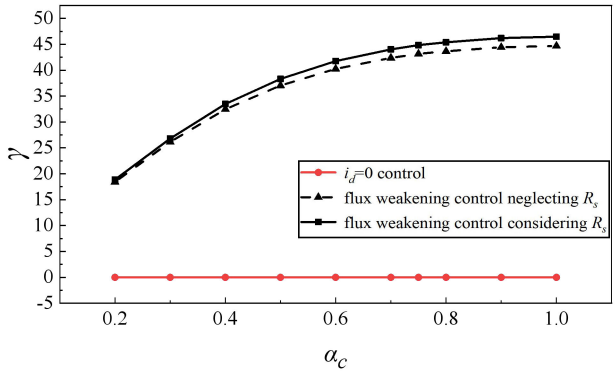


**FIGURE 20.** Current lead angle $\gamma$ at different $\alpha_c$.

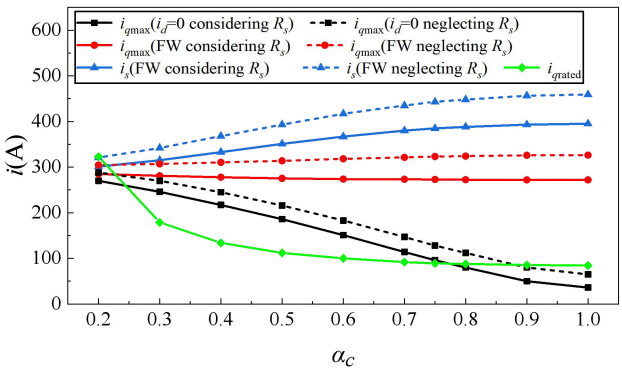


**FIGURE 21.** Maximum current curves at different $\alpha_c$.

FW control, $e_0$ and $i_{q\max}$ of the motor both increase with the increase of $h_M$, so the limiting output torque of the motor also keeps increasing, and the increasing trend gradually slows down. When the $h_M$ is too large, the rated torque cannot be output under $i_d = 0$ control.

According to the analysis of Fig. 15-18, when the $h_M$ increases, although the increase of $e_0$ and the decrease of $X_s$ are conducive to the improvement of the limiting output torque, the $i_{q\max}$ will decrease under $i_d = 0$ control due to the voltage limitation of the converter, while the $i_{q\max}$ will increase under FW control, as a result, under $i_d = 0$ control, the limiting output torque of the motor first increases and then decreases with the increase of the $h_M$, while under FW control, the limiting output torque of the motor keeps increasing with the increase of the $h_M$.

### C. THE EFFECT OF POLE ARC COEFFICIENT OF PM ON LIMITING OUTPUT TORQUE

$e_0$ and $X_s$ will change by adjusting the $\alpha_c$ of permanent magnet, while $R_s$ is unaffected. Fig. 19. shows the main parameter changes of the prototype when the $\alpha_c$ changes.

When the $\alpha_c$ increases, the excitation area of permanent magnet will increase, thus increasing the air gap flux, according to equation (15), this will lead to an increase in $e_0$. However, with the increase of $\alpha_c$, the distance between adjacent permanent magnets becomes smaller, which will lead to the increase of magnetic leakage between poles. Moreover, with the increase of air gap magnetic field, the degree of stator saturation will increase, as a result, the ability of air gap magnetic field to increase becomes smaller, so the increase trend of $e_0$ becomes slow. Different from increasing the $h_M$, increasing the $\alpha_c$ does not change the equivalent air gap length of the motor, but only improves the saturation degree of the core, therefore, $X_s$ will only slightly decrease with the increase of $\alpha_c$. In addition, current lead angle $\gamma$ at $i_{q\max}$ changes with the change of $\alpha_c$, as shown in Fig. 20. Under $i_d = 0$ control, the current lead angle $\gamma$ remains at 0°, while under FW control, the current lead angle $\gamma$ increases with the increase of the permanent magnet thickness. $\gamma$ also ends up approaching 47° and 45°, respectively, when resistance is considered and neglected.

When the $\alpha_c$ changes, the maximum current curves are shown in Fig. 21. It can be seen that under $i_d = 0$ control, the $i_{q\max}$ linearly decreases with the increase of the $\alpha_c$, while under FW control, $i_{q\max}$ slightly decreases, but $i_s$ increases with the increase of current lead angle $\gamma$ and the increase trend becomes slow. This trend is consistent with the change trend of $i_{q\max}$ in Fig. 5 and Fig. 8 when only $e_0$ is changed. Similar to the increase of $h_M$, with the increase of $\alpha_c$, the increase of air gap magnetic field makes the required $i_q$ at rated torque decrease, but with the deepening of saturation degree, the rated $i_q$ gradually becomes stable.

When the $\alpha_c$ changes, the limiting output torque curves are shown in Fig. 22. Similar to the increase of $h_M$, with the increase of the $\alpha_c$, the limiting output torque under the $i_d = 0$ control mode first increases and then decreases. This is also because $e_0$ of the motor increases and the speed slows down with the increase of the $\alpha_c$, while the $i_{q\max}$ of the motor decreases almost linearly. However, under the weak magnetic control, the $e_0$ of the motor increases and the $i_{q\max}$ decreases slightly, so the limiting output torque of the motor also keeps increasing, and the increasing trend becomes gradually slow. It is worth noting that when the $\alpha_c$ is too large, the motor also cannot output rated torque under the control of $i_d = 0$, while under FW control, the motor has also entered the FW zone when it outputs rated torque.

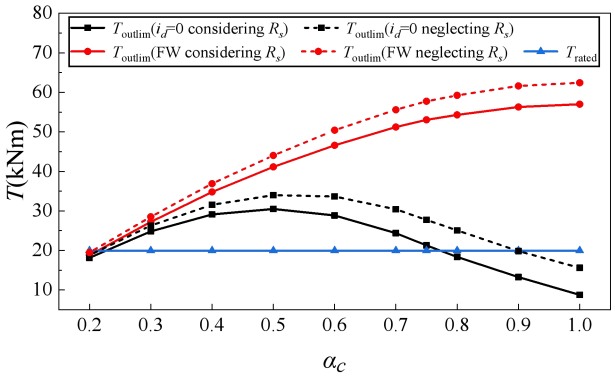


**FIGURE 22.** Limiting output torque curves at different $\alpha_c$.

When the $\alpha_c$ is increased, although the increase of $e_0$ is beneficial to improve the limiting output torque, the $i_{q\max}$ will decrease due to the voltage limitation of the frequency converter under $i_d = 0$ control, while the $i_{q\max}$ will decrease slightly under FW control, therefore, under $i_d = 0$ control, the limiting output torque of the motor first increases and then decreases with the increase of the $\alpha_c$. When the $\alpha_c$ is adjusted to make $e_0$ within the range of $0.75\sim0.85v_{\lim}$, the motor will obtain a larger limiting output torque. Under FW control, the limiting output torque of the motor increases with the increase of the $\alpha_c$.

### D. THE EFFECT OF LENGTH OF AIR-GAP ON LIMITING OUTPUT TORQUE

$e_0$ and $X_s$ will change by adjusting the $\delta$, but $R_s$ is unaffected. Fig. 23. shows the variation trend of the main electromagnetic parameters of the prototype when $\delta$ changes.

When the $\delta$ increases, the reluctance of the main magnetic circuit will increase accordingly, so the magnetic flux of the air gap will become smaller. As can be seen from equation (15), this will lead to the decrease of $e_0$. Moreover, when the motor is under the no-loaded state, the air gap reluctance accounts for a major part of the main reluctance, which is proportional to $\delta$, so $e_0$ decreases linearly with the increase of the $\delta$. Besides, the specific permeability of the main magnetic circuit $\lambda_m$ is inversely proportional to $\delta$,

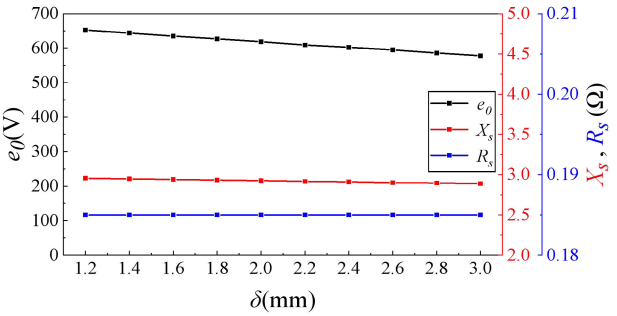


**FIGURE 23.** $e_0$, $R_s$, $X_s$ at different $\delta$.

so the $\lambda_m$ will decrease when the $\delta$ increases. According to equation (17), this will lead to a linear decrease of the $X_s$ of the motor, but the saturation degree of the stator teeth will decrease with the increase of the $\delta$, making the $X_s$ slightly increase. However, compared with the influence of the increase of $\delta$ on $\lambda_m$, the saturation degree has a relatively small influence on $\lambda_m$. In the end, the combined effect of the two results in the slight decrease of $X_s$ with the increase of the $\delta$. When the $\delta$ changes, the current lead angle $\gamma$ at $i_{q\max}$ is shown in Fig. 24.

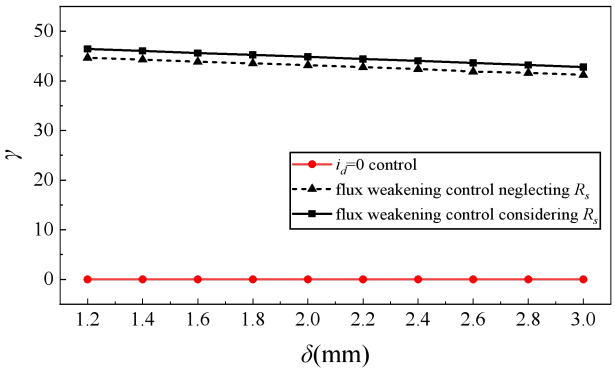


**FIGURE 24.** Current lead angle $\gamma$ at different $\delta$.

Under $i_d = 0$ control, the current lead angle $\gamma$ remains at 0°, while under FW control, the current lead angle $\gamma$ decreases with the increase of $\delta$, this is caused by the decrease of $e_0$, and the trend of decreasing $\gamma$ is consistent with the trend of decreasing $e_0$, which is a linear decrease. When the $\delta$ is small and $e_0$ is close to $v_{\lim}$, the current lead angle $\gamma$ in the case of considering resistance is still close to 47°, while the current lead angle in the case of ignoring resistance is still close to 45°.

When the $\delta$ changes, the maximum current curves are shown in Fig. 26. It can be seen that under $i_d = 0$ control, the $i_{q\max}$ increases with the increase of $\delta$, this is because when the $\delta$ increases, the decrease of $e_0$ will make the difference between $v_{\lim}$ and $e_0$ larger, so more current can be input. While under FW control, $e_0$ and $X_s$ decrease with the increase of $\delta$. According to equation (5), this will cause the radius of the voltage limit circle to slightly decrease and the center of

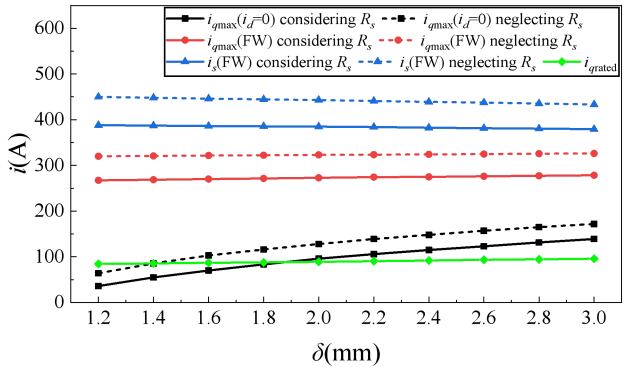


**FIGURE 25.** Maximum current curves at different $\delta$.

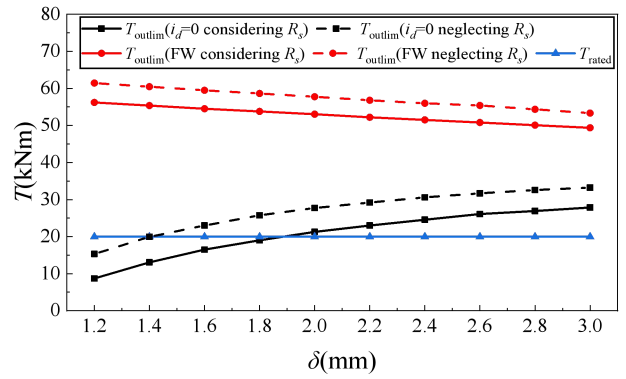


**FIGURE 26.** Limiting output torque curves at different $\delta$.

the circle to slightly move upward, which leads to the slight increase of $i_{q\max}$ with the increase of the $\delta$. However, the current lead angle $\gamma$ decreases with the increase of the $\delta$, resulting in the decrease of id corresponding to $i_{q\max}$.

When the $\delta$ changes, the limiting output torque curves are shown in Fig. 26. With the increase of $\delta$, under the control of $i_d$, although $e_0$ decreases, the limiting output torque also tends to increase because $i_{q\max}$ increases at a higher rate. However, under the FW control strategy, when $e_0$ decreases, the $i_{q\max}$ increases at a slower rate, so the limiting output torque eventually presents a downward trend. It is worth noting that when the $\delta$ is too small, the rated torque cannot be output by using $i_d = 0$ control.

According to the analysis of Fig. 23-26, when the $\delta$ increases, the decrease of $e_0$ is not conducive to improving the limiting output torque. However, under the $i_d = 0$ control, the increase of $i_{q\max}$ and the decrease of $X_s$ are both conducive to improving the limiting output torque, which generally results in the increase of the limiting output torque with the increase of the $\delta$. However, under the FW control, $i_{q\max}$ and $e_0$ decrease with the increase of $\delta$, which is not conducive to the improvement of limiting output torque, therefore, the limiting output torque decreases with the increase of $\delta$. However, the $i_{q\max}$ under the FW control is always greater than that under $i_d = 0$ control, therefore, the limiting output torque under the FW control is greater than that under the

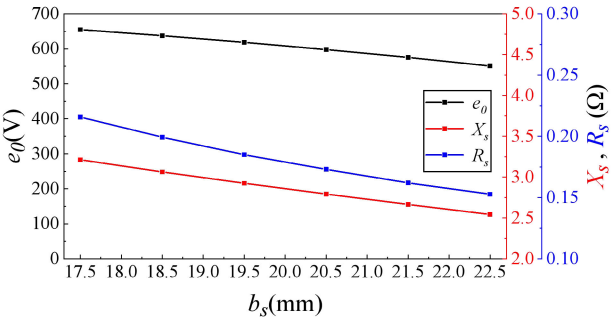


**FIGURE 27.** $e_0$, $R_s$, $X_s$ at different $b_s$.

$i_d = 0$ control, however, the difference between the them becomes smaller as the $\delta$ increases.

### E. THE EFFECT OF SLOT WIDTH ON LIMITING OUTPUT TORQUE

Adjusting the $b_s$ of the stator will simultaneously change $e_0$, $R_s$, and $X_s$. Fig. 27. shows the variation trend of the main electromagnetic parameters of the prototype when $b_s$ changes.

When the $b_s$ increases, the increase of tooth magnetic density will lead to the increase of the reluctance of the main magnetic circuit, so the air gap magnetic flux will become smaller. According to equation (15), this will lead to the decrease of $e_0$. In addition, when the $b_s$ increases, the degree of saturation of the core becomes higher, which will lead to the decrease of $X_s$ of the motor. With the increase of $b_s$, in order to meet the appropriate slot filling rate, the copper wire thickness $h_1$ remains unchanged, but the copper wire width $k_1$ will increase accordingly, which will lead to the increase of the cross-sectional area of each turn winding. According to equation (16), $R_s$ will decreases approximately linearly. When the $b_s$ changes, the current lead angle $\gamma$ at $i_{q\max}$ is shown in Fig. 28.

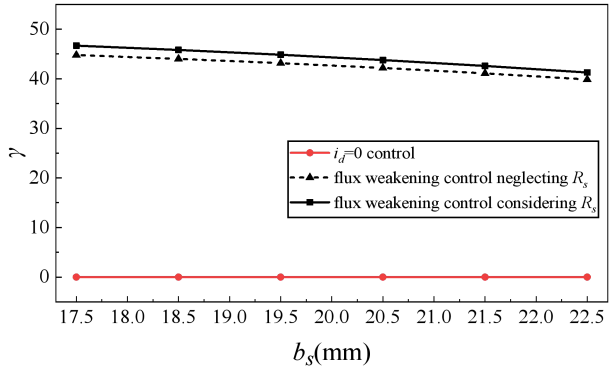


**FIGURE 28.** Current lead angle $\gamma$ at different $b_s$.

Under $i_d = 0$ control, the current lead angle $\gamma$ remains at 0°, while under FW control, the current lead angle $\gamma$ decreases with the increase of $b_s$, this is also due to the decrease of $e_0$, and the trend of decreasing $\gamma$ is consistent with

the trend of decreasing $e_0$, which is a linear decrease. When $b_s$ is small and $e_0$ approaches $v_{\text{lim}}$, the current lead angle $\gamma$ in the case of considering resistance is still close to 47°, while the current lead angle in the case of ignoring resistance is still close to 45°.

When the $b_s$ changes, the maximum current curves are shown in Fig. 29. It can be seen that under both control strategies, $i_{q\max}$ increases as $b_s$ increases, and larger current can be obtained when resistance is ignored under both control strategies. According to equations (9) and (12), since $e_0$, $X_s$ and $R_s$ all decrease with the increase of $b_s$, their decrease is conducive to increasing the inputable $i_{q\max}$ of the SMPMSM. The current lead angle $\gamma$ decreases with the increase of $b_s$, so $i_s$ also increases with the increase of $i_{q\max}$. In addition, it is worth noting that with the increase of $b_s$, the magnetic reluctance of the magnetic circuit increases, resulting in the increase of the $i_{q\text{rated}}$ required for output rated torque. However, due to the decrease of resistance, the thermal load at the rated operating point of the SMPMSM hardly changes. The trend of current variation in Fig. 29. is consistent with that in Fig. 5. and Fig. 8.

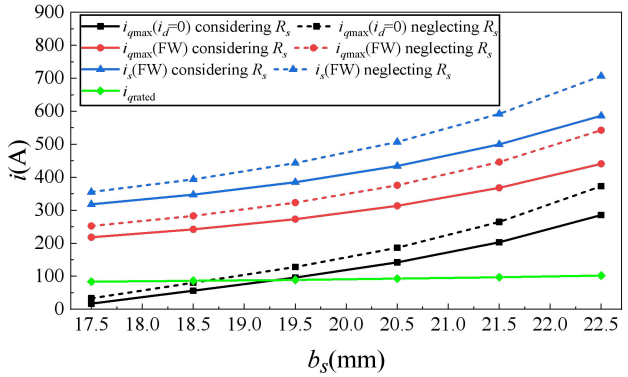


**FIGURE 29.** Maximum current curves at different $b_s$.

When the $b_s$ changes, the limiting output torque curves are shown in Fig. 30. With the increase of $b_s$, although the decrease of $e_0$ is not conducive to the improvement of limiting output torque, $i_{q\max}$ increases under both control strategies, and its increase rate is greater than the decrease rate of $e_0$, therefore, the limiting output torque increases with the increase of $b_s$ under both control strategies. In addition, the increase rate of $i_{q\max}$ is larger under the $i_d = 0$ control, so the limiting output torque increases faster under this control strategy. It is also worth noting that when $b_s$ is too small, it is difficult for the SMPMSM to output the rated torque under the $i_d = 0$ control. The variation trend of the torque in Fig. 30. is consistent with that in Fig. 6. and Fig. 9.

According to the analysis in Fig.27-30, with the increase of $b_s$, although $e_0$ tends to decrease, the increase of $R_s$, $X_s$ and $i_{q\max}$ is conducive to the increase of limiting output torque under the two control strategies, as a result, the limiting output torque of the SMPMSM increases with the increase of $b_s$ under the two control strategies, moreover, under the

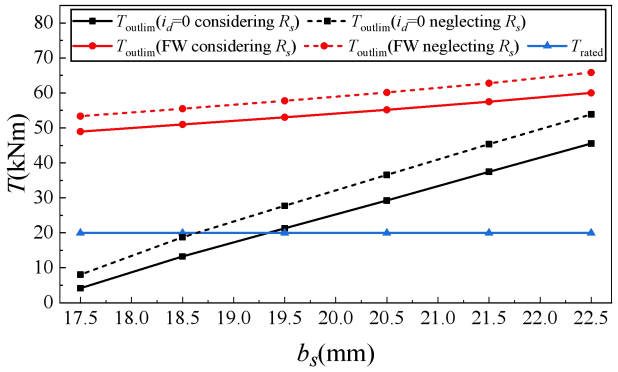


**FIGURE 30.** Limiting output torque curves at different $b_s$.

$i_d = 0$ control, the increase rate of limiting output torque is larger. In addition, it is worth noting that increasing the slot depth has a similar influence rule on the main electromagnetic parameters of the SMPMSM as increasing the slot width, so there should also be a similar variation rule of the $i_{q\max}$ and the limiting output torque, so it will not be covered again in this paper.

## V. EXPERIMENTAL VALIDATION

The finite element method was used to analyze the influence of various parameters of the SMPMSM on the limiting output torque. In order to prove the correctness of the finite element results, the limiting output torque experiment was carried out on the prototype in Table 1 under the two control strategies. If the experiment only tests the limit point of the torque, the experimental results are too few to better prove the correctness of the finite element results, therefore, the prototype output torque at various currents are tested in the experiment, including the limit output torque at the limit current.The stator, rotor and test platform of the prototype are shown in Fig. 31. The inner rotor motor can directly connect the shaft with the test motor through the torque analyzer to carry out torque test. However, due to the structural characteristics of the external rotor motor, a belt is used to connect the prototype to a mechanical roller, which is directly connected to the rotating shaft of the load motor. The torque test device is shown in Fig. 32. A moment arm is installed at one end of the stator shaft. The moment arm and the stator shaft are connected by a key, so that the torque on the stator shaft can act on the moment arm bar rather than the support seat, and the pressure sensor is installed below the moment arm. According to the principle of force and reaction force, the torque output by the rotor will also react on the stator and be transferred to the pressure sensor through the moment arm. The output torque of the motor can be calculated by equation (18).

$$T = F \times r \tag{18}$$

where $T$ is the output torque of the SMPMSM, $F$ is the pressure value measured by the pressure sensor, and $r$ is the length of the moment arm.

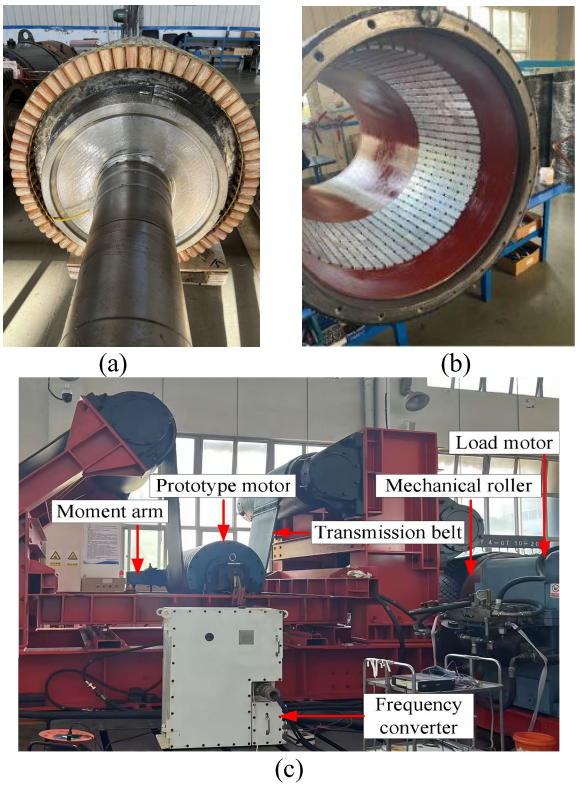


**FIGURE 31.** Prototype experiment (a) Stator (b) Rotor (c) Experiment platform.

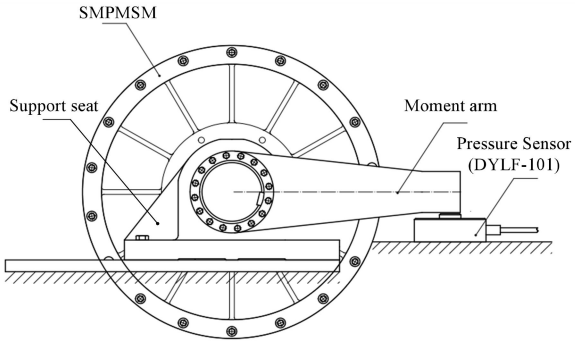


**FIGURE 32.** Torque testing device.

Some parameters for the operation of the experiment are shown in Table 2.

Under $i_d = 0$ control, turn off the FW control option of the converter to keep its output current lead angle always at 0°. After starting the prototype to the rated speed, then gradually load the test motor until the speed of the prototype decreases and the frequency converter prompts an over-voltage fault. In order to ensure the accuracy of the experimental data, record the experimental data every time the input current of the prototype is increased by 5A. Under the FW control, turn on the FW control option of the frequency converter, so that it can adjust the current lead angle according to the operating state of the SMPMSM, and repeat the above loading

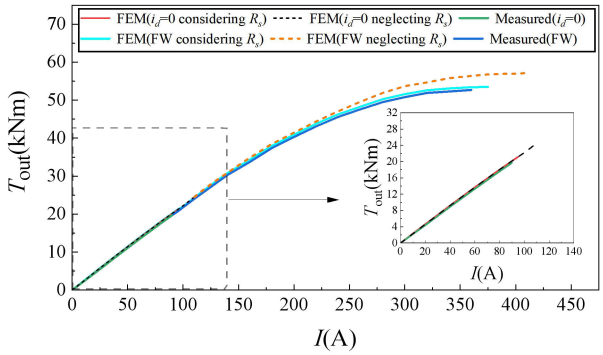


**FIGURE 33.** Comparison of FEM and measured results.

**TABLE 2.** Parameters for the operation of the experiment.

| Item | Unit | Value |
|---|---|---|
| Converter power | kW | 630 |
| Output frequency of converter | Hz | 38.25 |
| Carrier frequency of converter | kHz | 4 |
| Duty cycle of converter | - | 70% |
| Output voltage limit of converter | V | 1140 |
| Sampling frequency of pressure sensor | Hz | 10 |
| Load motor power | kW | 560 |

operation. It should be noted that under the FW control, when the load is small, the frequency converter will also run in $i_d = 0$ mode. Only when the load increases to a certain extent and the terminal voltage of the motor exceeds the limit value in the control mode of $i_d = 0$, the frequency converter will increase the current lead angle and enter the weak magnetic region to maintain the motor operation. Therefore, under the low current, the experimental curve under the FW control coincides with $i_d = 0$ control. The comparison between test results and simulation results are shown below.

As can be seen from Fig. 33. In the experiment, when the current reaches 90A, the control strategy is transformed from $i_d = 0$ to FW, and the output torque of the motor is 19.7kNm at this time. In the FEM, the control strategy is changed when the current reached 95A, and the output torque of the motor is 21.2kNm. Under the FW control strategy, when the current reaches 360A and the output torque is 52.7kNm, the motor starts to stall, and the converter stops, while in the FEM, the motor can obtain the limit output torque of 54kNm at 375A current. Output torque at various currents of the prototype are in good agreement with the FEM results considering resistance, which proves that the finite element results of limiting output torque mentioned above are correct. But, due to the influence of iron loss, stray loss and the inevitable voltage drop of the converter element, the test results are slightly lower than the FEM results, and the test results of the motor maximum current under $i_d = 0$ control and FW control are also slightly lower than the FEM results.

However, there is a large error between the test results and the FEM results neglecting resistance, which indicates that the winding resistance has a certain influence on the limiting output capacity of this kind of motor, so the resistance should be considered.

Considering that the SMPMSM in this paper runs under the rated operating point for a long time, and the overload is only occasional and short time, in order to maximize current utilization and reduce motor temperature rise, the rated operating point of the motor should be designed near the voltage limit value under the $i_d = 0$ control, the test results show that the prototype meets this requirement. In addition, in industrial applications, the capacity of the converter matched with the SMPMSM is generally 1.2 times the rated power of the SMPMSM, considering that the maximum output current of the converter is 1.8 times its rated current, that is, the maximum output current of the converter matched with the prototype is about 230A, according to the test, under this current, the output torque of the motor is 44kNm, about 2.2 times the rated torque, which just meets the requirements of the belt conveyor for its drive motor. Therefore, it can be proved that the prototype parameters in Table 1 are relatively optimized results. The experimental results prove the correctness of the theoretical analysis in the paper.

## VI. CONCLUSION

In this paper, the limiting output capacity of low-speed and high-torque SMPMSM is studied considering the voltage limit of converter and the resistance voltage drop. By analyzing the expression of output torque of SMPMSM, the influence of electromagnetic parameters such as $e_0$, $R_s$, and $X_s$ on the limiting $i_q$ and limiting output torque of SMPMSM operating at constant speed under voltage limit is derived under the two control strategies. On the basis of the prototype, the FEM is used to analyze the effects of the number of turns of the motor winding, the thickness and the polar arc coefficient of permanent magnet on the limiting output capacity of SMPMSM under the two control strategies. The correctness of the finite element analysis is verified by the prototype experiment, and the following conclusions can be obtained through the finite element analysis:

(1) Under $i_d = 0$ and FW control, the limiting output capacity of the SMPMSM can be significantly improved by reducing the number of winding turns, and the thermal load of the SMPMSM hardly changes at the rated operating point. Therefore, the number of winding turns can be determined according to the demand of the limiting output torque and the capacity of the converter.

(2) Under $i_d = 0$ control, with the increase of the thickness of PM, the limiting output capacity of SMPMSM will first increase and then decrease. When the thickness of PM are too large which causes $e_0$ exceed $0.9v_{\lim}$, the SMPMSM cannot output the rated torque. When $e_0$ is within the range of $0.75\sim0.85v_{\lim}$ by adjusting the thickness of PM, the SMPMSM can achieve a larger limiting output capacity. While, under the FW control, the limiting output capacity of SMPMSM will continue to increase with the increase of the thickness of the PM, but the increasing trend gradually decreases. In addition, with the increase of the thickness of the PM, the motor has entered the FW zone at the rated operating point, which will lead to higher temperature rise at the rated operating point. According to the FEM results, when $e_0$ is designed around $0.9v_{\lim}$ by changing the thickness of the PM, the SMPMSM can obtain both larger limiting output capacity and lower temperature rise at the operating point. In addition, the influence of the polar arc coefficient of PM on the limiting output capacity of SMPMSM is almost identical to that of the thickness of PM, and they have similar conclusions.

(3) Under $i_d = 0$ control, with the increase of the air-gap length, SMPMSM can input a larger $i_{q\max}$, so the limiting output capacity of SMPMSM will increase. While, under FW control, as the air-gap length increases, the $e_0$ and the inputable $i_{q\max}$ of SMPMSM decrease at the same time, as a result, the limiting output capacity of SMPMSM shows a decreasing trend.

(4) Under $i_d = 0$ and FW control, the limiting output capacity of the SMPMSM can be improved by increasing slot width, and it is more significantly under $i_d = 0$ control. Moreover, the thermal load of the SMPMSM hardly changes at the rated point. Therefore, for SMPMSM with high limiting output capacity requirements, the slot width should be increased as far as possible under the premise of satisfying the mechanical strength. In addition, the influence trend of slot depth on the limiting output capacity of SMPMSM is similar to that of slot width.

## REFERENCES

[1] B. Gan, B. Zhang, Q. Li, F. Guihong, and G. Li, "Research on operation of low-speed and high-torque module combined stator permanent magnetic fault-tolerant motor with unequal span winding," *IEEE Access*, vol. 8, pp. 166824–166838, 2020.

[2] Z. Liu, Y. Hu, J. Wu, B. Zhang, and G. Feng, "A novel modular permanent magnet-assisted synchronous reluctance motor," *IEEE Access*, vol. 9, pp. 19947–19959, 2021.

[3] J.-C. Son, J.-Y. Kim, J.-W. Choi, D.-K. Lim, and H.-K. Yeo, "Performance enhancement of the IPMSM for HEV applications using grain-oriented electrical steel and design optimization," *IEEE Access*, vol. 10, pp. 46599–46607, 2022.

[4] C. Cavallaro, A. O. D. Tommaso, and R. Miceli, "Efficiency enhancement of permanent-magnet synchronous motor drives by online loss minimization approaches," *IEEE Trans. Ind. Electron.*, vol. 52, no. 4, pp. 1153–1160, Aug. 2005.

[5] D. Fodorean, L. Idoumghar, M. Brevilliers, P. Minciunescu, and C. Irimia, "Hybrid differential evolution algorithm employed for the optimum design of a high-speed PMSM used for EV propulsion," *IEEE Trans. Ind. Electron.*, vol. 64, no. 12, pp. 9824–9833, Dec. 2017.

[6] D. Mohan, X. Zhang, and G. H. B. Foo, "Three-level inverter-fed direct torque control of IPMSM with constant switching frequency and torque ripple reduction," *IEEE Trans. Ind. Electron.*, vol. 63, no. 12, pp. 7908–7918, Dec. 2016.

[7] K. T. Chau, C. C. Chan, and C. Liu, "Overview of permanent-magnet brushless drives for electric and hybrid electric vehicles," *IEEE Trans. Ind. Electron.*, vol. 55, no. 6, pp. 2246–2257, Jun. 2008.

[8] C. Ma, C. Chen, Q. Li, H. Gao, Q. Kang, J. Fang, H. Cui, K. Teng, and X. Lv, "Analytical calculation of no-load magnetic field of external rotor permanent magnet brushless direct current motor used as in-wheel motor of electric vehicle," *IEEE Trans. Magn.*, vol. 54, no. 4, pp. 1–6, Apr. 2018.
[9] S. Zuo, F. Lin, and X. Wu, "Noise analysis, calculation, and reduction of external rotor permanent-magnet synchronous motor," *IEEE Trans. Ind. Electron.*, vol. 62, no. 10, pp. 6204–6212, Oct. 2015.
[10] J. Zhang, B. Zhang, G. Feng, and B. Gan, "Design and analysis of a low-speed and high-torque dual-stator permanent magnet motor with inner enhanced torque," *IEEE Access*, vol. 8, pp. 182984–182995, 2020.
[11] J. Wu, Y. Hu, B. Zhang, G. Feng, and Z. Liu, "Comparison and analysis of different rotor structures of double-stator permanent magnet synchronous motor," *IET Electr. Power Appl.*, vol. 16, no. 6, pp. 685–700, Jun. 2022.
[12] T. Vajsz and L. Számel, "Overload-capability analysis of PMSM servo- and robot-drives using DTC-SVM methods: Part 1," in *Proc. IEEE 18th Int. Power Electron. Motion Control Conf. (PEMC)*, Aug. 2018, pp. 730–736.
[13] T. Vajsz and L. Számel, "Overload-capability analysis of PMSM servo- and robot-drives using DTC-SVM methods: Part 2," in *Proc. IEEE 18th Int. Power Electron. Motion Control Conf. (PEMC)*, Aug. 2018, pp. 737–743.
[14] A. Sanz, E. Oyarbide, R. Gálvez, C. Bernal, P. Molina, and I. San Vicente, "Analytical maximum torque per volt control strategy of an interior permanent magnet synchronous motor with very low battery voltage," *IET Electr. Power Appl.*, vol. 13, no. 7, pp. 1042–1050, Jul. 2019.
[15] C. Miguel-Espinar, D. Heredero-Peris, G. Gross, M. Llonch-Masachs, and D. Montesinos-Miracle, "Maximum torque per voltage flux-weakening strategy with speed limiter for PMSM drives," *IEEE Trans. Ind. Electron.*, vol. 68, no. 10, pp. 9254–9264, Oct. 2021.
[16] Z. Shi, X. Sun, Y. Cai, X. Tian, and L. Chen, "Design optimisation of an outer-rotor permanent magnet synchronous hub motor for a low-speed campus patrol EV," *IET Electr. Power Appl.*, vol. 14, no. 11, pp. 2111–2118, Nov. 2020.
[17] C. Babetto, G. Berardi, N. Bianchi, and G. Benedetti, "Design and optimization of synchronous motors for low-voltage electric vehicles," in *Proc. IEEE Energy Convers. Congr. Expo. (ECCE)*, Sep. 2019, pp. 6070–6077.
[18] R. Leuzzi, P. Cagnetta, S. Ferrari, P. Pescetto, G. Pellegrino, and F. Cupertino, "Transient overload characteristics of PM-assisted synchronous reluctance machines, including sensorless control feasibility," *IEEE Trans. Ind. Appl.*, vol. 55, no. 3, pp. 2637–2648, May 2019.
[19] W. Zhao, F. Zhao, T. A. Lipo, and B.-I. Kwon, "Optimal design of a novel V-type interior permanent magnet motor with assisted barriers for the improvement of torque characteristics," *IEEE Trans. Magn.*, vol. 50, no. 11, pp. 1–4, Nov. 2014.
[20] F. Birnkammer and D. Gerling, "Influence of machine parameters and cooling method on the overload capability of permanent magnet synchronous machines," in *Proc. 21st Int. Conf. Electr. Mach. Syst. (ICEMS)*, Oct. 2018, pp. 16–20.
[21] H. Liu, R. Wrobel, S. Ayat, and C. Zhang, "Coupled electromagnetic and thermal design-optimisation of a traction IPM machine with high-torque overload capability," in *Proc. 13th Int. Conf. Electr. Mach. (ICEM)*, Sep. 2018, pp. 2647–2653.
[22] S.-M. Sue and C.-T. Pan, "Voltage-constraint-tracking-based field-weakening control of IPM synchronous motor drives," *IEEE Trans. Ind. Electron.*, vol. 55, no. 1, pp. 340–347, Jan. 2008.
[23] G. Feng, C. Lai, X. Tan, and N. C. Kar, "Maximum-torque-per-square-ampere control for interior PMSMs considering cross-saturation inductances," *IEEE Trans. Transport. Electrific.*, vol. 7, no. 3, pp. 1482–1492, Sep. 2021.

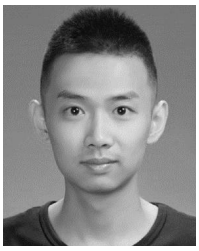

**JIACHENG WU** received the B.S. and master's degrees in electrical engineering and automation from the Shenyang University of Technology, Shenyang, China, in 2015 and 2020, respectively, where he is currently pursuing the Ph.D. degree in electrical engineering. His current research interest includes the design and control of permanent magnet motors.

**GUIHONG FENG** received the master's degree from Northeast University. She is currently a Professor of electrical engineering with the Shenyang University of Technology. Her current research interest includes motors and its control.

**YAN HU** received the Ph.D. degree in electrical engineering from the Shenyang University of Technology.

From 2004 to 2020, she is the Director of the Electrical Engineering Department, Shenyang University of Technology, and the Director of the Institute of Motion Control Motor. She is the Executive Director of the electromagnetic field teaching with the Teaching Materials Research Association of Chinese colleges and universities. Her current research interests include special motors and its control and numerical analysis of the electromagnetic field.

**BINGYI ZHANG** received the Ph.D. degree in electrical engineering from the Shenyang University of Technology. He is currently a Senior Electrical Bid Evaluation Expert of the China International Tendering Corporation. His current research interest includes motors and its control. He is a member of the China Electrical Engineering Society and IEEE-IAS.

**ZEYU LIU** received the B.S. degree in electrical engineering and automation from the Shenyang University of Technology, Shenyang, China, in 2017, where he is currently pursuing the Ph.D. degree in electrical engineering. His current research interest includes the design and control of permanent magnet motors.